Journal of Applied Fluid Mechanics, Vol. 17, No. 7, pp. 1485-1498, 2024.
Available online at www.jafmonline.net, ISSN 1735-3572, EISSN 1735-3645.
https://doi.org/10.47176/jafm.17.7.2424

Analysis of Flow-induced Noise Characteristics of Ethylene Cracking Furnace Tubes before and after Coking

F. Q. Zhou[1,2†], S. Y. Zhao[1,2], S. J. Zhang[1,2], Y. Zhang[3], S. C. Fu[1,2] and S. Q. Yu[4]

[1] *School of Mechanical Engineering and Rail Transit, Changzhou University, Changzhou 213164, Jiangsu, China*
[2] *Jiangsu Key Laboratory of Green Process Equipment, Changzhou 213164, Jiangsu, China*
[3] *School of Safety Science and Engineering, Changzhou University, Changzhou 213164, Jiangsu, China*
[4] *Wuxi Liai Machinery Manufacturing Co., Ltd., Wuxi 214111, Jiangsu, China*

†Corresponding Author Email: zhoufaqi@cczu.edu.cn

ABSTRACT

This paper presents a comprehensive investigation of flow-induced noise characteristics in ethylene cracking furnace tubes, covering both pre- and post-coking conditions. Large-eddy simulation (LES) was employed in conjunction with a generalized Lighthill's acoustic analogy model. The results indicate that noise sources can be classified as dipole acoustic sources, with energy primarily concentrated ranged from 300 to 1500 Hz, in comparison to standard conditions. The primary location of the acoustic source was identified in the region commonly referred to as the "necking" of the furnace tube, demonstrating a strong correlation with turbulence intensity near the tube wall. As the coke layer thickness in the furnace tube increased from 5 mm to 15 mm, both the sound power level and turbulence intensity exhibited significant growth. Specifically, the sound power level increased by 60.5% while the turbulence intensity increased by 58.5%. Variations in the overall sound pressure level (OASPL) curve measured within the tube could be utilized to assess coking levels. Significant peaks in the OASPL curve were observed as the furnace tube underwent substantial coking, with coke layer thicknesses of 10 mm and 15 mm. The corresponding OASPL values recorded were 79.25 dB and 119.08 dB, respectively. The findings of this work offer significant insights that may contribute to enhanced safety measures in the operation of ethylene cracking furnace tubes.

Article History

Received November 8, 2023
Revised February 11, 2024
Accepted February 14, 2024
Available online April 30, 2024

Keywords:

Coke deposition
Flow-induced noise characteristics
Numerical simulation
Pressure pulsation
Turbulence intensity

1. INTRODUCTION

The stable operation of ethylene cracking furnaces holds paramount importance in polymer and compound production (Fakhroleslam & Sadrameil, 2020; IEA, 2021; Chen et al., 2023). However, coke deposition commonly occurs on the inner walls of furnace tubes during the thermal cracking process, impacting process performance and safety in petrochemical operations (Tari et al., 2009; Han et al., 2019). Currently, effective methods for predicting coke deposition in furnace tubes are still lacking (Pan & Lan, 2016; Solaimany et al., 2016; Su et al., 2016; Valus et al., 2017; Ren et al., 2020; Wei, 2020). Studies have indicated that coke deposition in the furnace tube alters the flow channel structure, thereby affecting the flow and acoustic field characteristics within the tube (Mahamulkar et al., 2016; Coombs et al., 2020). Analyzing the flow-induced noise characteristics of furnace tubes before and after coking can provide a crucial reference for predicting equipment failure.

In recent decades, research concerning ethylene cracking furnace tubes has primarily focused on operational parameters, thermodynamic properties, and noise. Zhang et al. (2013) utilized eddy dissipation and computational fluid dynamics (CFD) to explore the effects of raw material feed rate, reaction tube wall temperature, and heat flux on process performance. Their findings indicated a positive impact of the wall temperature profile and reaction tube heat flux profile on the production of pyrolysis products. Subsequently, Barik et al. (2016) established a connection between heat transfer effects in a furnace tube and the Reynolds number, proposing the use of nanofluids to enhance convection in the tube and improve heat transfer. The heat transfer effects of U-shaped and 90° elbow furnace tubes were compared by Haldar and Shukla (2017) using the k-ε equation, revealing that greater bending angles result in heightened heat

NOMENCLATURE

C_s	Smagorinsky constant	T_{ij}	Lighthill's stress tensor
CFL	Courant number	t	simulation time
c_0	sound velocity	Δt	time step
D	furnace tube outer diameter	U	magnitude of the flow velocity through the cell
D_{in}	furnace tube inner diameter	$\bar{u}_i$	fluid velocity components in physical space of i direction
d	distance to the closest wall	$\bar{u}_j$	fluid velocity components in physical space of j direction
d_{out}	coking furnace tube inner diameter	V	volume of the computational cell
f_{max}	maximum acoustic frequency	x_i	physical space i direction
h	coke layer thickness	x_j	physical space j direction
G	Green function	Δx	cell size in the flow direction
k	Von Karman constant	μ_t	subgrid-scale turbulent viscosity
L	furnace tube length	ρ	density of the fluid
L_s	mixing length for subgrid scales	ρ'	density disturbance caused by sound
l_g	length of the growth zone in the furnace tube	δ_{ij}	Kronecker Delta symbol
l_m	length of the mature zone in the furnace tube	υ	kinematic viscosity
l_o	length of the origin zone in the furnace tube	τ	acoustic emission time at the sound source
p	the static pressure	τ_{ij}	subgrid-scale stress
$\bar{S}_{ij}$	rate-of-strain tensor for the resolved scale	τ_{kk}	isotropic part of the subgrid-scale stresses

transfer. Further exploration by Mohammed (2018) revealed characteristics of incompressible flow within U-shaped furnace tubes with varying curvature radii, where heat transfer increased with curvature radius; however, the effects of coking were not taken into account. Amini et al. (2022) simulated heat transfer and thermal oil flow in a radiant coil section, accounting for coke formation within the coil, using the k-ε equation. Their results demonstrated that coke deposition reduces the flow area of the coil and elevates fluid velocity, but decreases heat transfer efficiency. Zhang et al. (2023) utilized LES and generalized Lighthill's acoustic analogy modeling to analyze the impact of coke deposition with different heights and attack angles on a tube, specifically concerning flow-induced noise. They observed proportionality between the OSPL of the noise and the rate of coke growth.

While research on flow-induced noise characteristics in cracking furnace tubes is relatively limited, the studies referenced here involve tube noise models, which provide valuable insights. Pittard et al. (2004), for example, investigated tube noise using a hybrid approach that combines experimental methods with numerical simulations; they found that inlet velocity significantly impacts noise. Mori et al. (2017) explored the acoustic characteristics of T-shaped rectangular cross-section pipes with different wall thicknesses using utilizing LES and boundary element method (BEM) models, identifying significant flow-induced noise characteristics, particularly with 2 mm wall thickness. However, the computational cost of this approach was overlooked. Paul et al. (2018) predicted pressure wave propagation from a noise source to a cylinder using LES and Lighthill's acoustic analogy models, highlighting the efficiency and cost-effectiveness of this approach compared to LES and BEM methods. Han et al. (2020) numerically analyzed flow-induced noise characteristics in natural gas manifolds with a combination of LES and Ffowcs Williams-Hawkings (FW-H), and proposed effective noise-reduction measures accordingly; however, the acoustic mechanism was not clarified. Murugu et al. (2022) used unsteady Reynolds-averaged Navier-Stokes (URANS) and LES methods to simulate the acoustics of a chevron nozzle compressible jet, revealing close agreement between LES predictions and experimental data while URANS underestimated both the flow field and sound pressure level. Lv et al. (2023) used LES and FW-H models to predict the flow-induced noise of a T-type deceleration tee tube, identifying severe pressure pulsation as the primary source of flow-induced noise, but neglecting the effect of the solid boundary at the branch tube on noise.

The flow-induced noise of a furnace tube before and after coking was investigated in this study using LES and a generalized Lighthill's acoustic analogy model. The influence of coke layer thickness in the furnace tube on the flow-induced noise is investigated, providing essential data for predicting furnace tube coking and eliminating safety hazards. Additionally, the findings offer valuable insights into noise control for related industrial equipment, which may significantly benefit the sustainable development of the petrochemical industry.

2. PHYSICAL MODEL AND SIMPLIFICATION PROCESS

This paper focuses on a radiation coil section in the millisecond cracking furnace of a petrochemical company, as illustrated in Fig. 1(a). Compared with other types of radiant coils, this furnace tube has advantages including a lack of elbows, high heat transfer efficiency, low pressure-drop, and rapid cracking reaction. However, its drawbacks-primarily its propensity for rapid coke layer formation on the furnace tube's inner wall-necessitate mitigation measures, chiefly frequent and swift coke removal (Jakobi, & Gommans, 2007; Rossi et al., 2019).

Upon examining the fractured-failed furnace tube in Fig. 1(b), it becomes evident that the coke layer's thickness closely resembles that of the furnace tube wall.

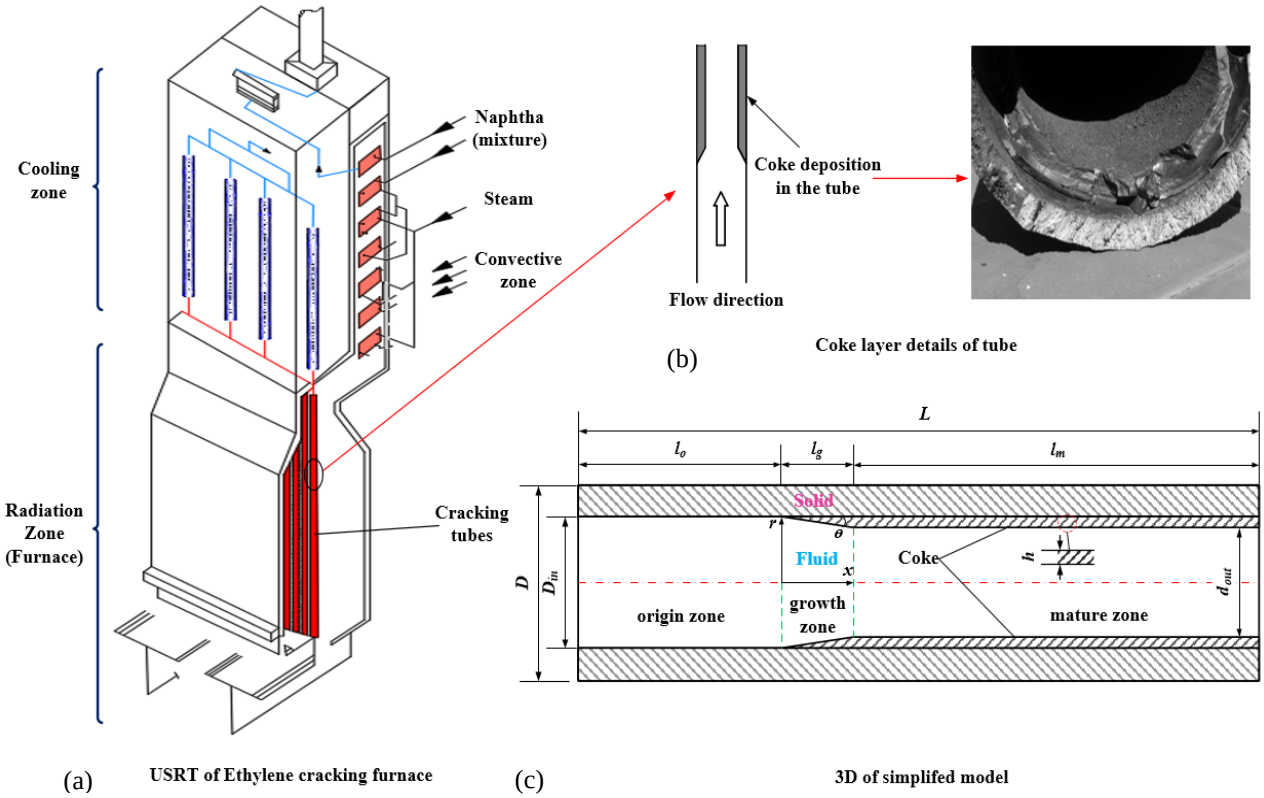

Fig. 1 Furnace tubes coking model and simplification process

The coke layer exhibits a smooth and sturdy texture with low porosity. Due to the absence of industrial measurement data concerning coke layer thickness in furnace tubes, and for the sake of simplicity, simplifications for the coked tube are made here with reference to the literature: surface irregulatrities on the coke layer are disregarded, and it is assumed to be flat and uniform (Amini et al., 2022). The area near the inlet end of the furnace tube, where the coke layer has not yet formed, is designated as the origin zone. The section near the central left end of the tube, where the coke layer gradually increases in thickness, is termed the growth zone. Finally, the portion close to the outlet end of the furnace tube, where the thickness of the coke layer on the inner wall progressively rises until reaching a predetermined value, is identified as the mature zone (Fig. 1(c)).

3. NUMERICAL MODELS

A hybrid numerical method was utilized in this study to predict the flow-induced noise of the ethylene cracking furnace tube before and after coking, as illustrated in Fig. 2. LES was employed to solve the unsteady flow field, extracting characteristic parameters such as velocity, pressure, and density. Subsequently, aided by the iCFD module in Actran, the characteristic parameters of the unsteady flow were mapped to the acoustic field simulation. Acoustic prediction was executed through interpolation between the CFD grid and the finite element grid. Finally, the time-domain acoustic source was subjected to discrete Fourier transform (DFT), and the flow-induced noise and propagation characteristics were solved using the direct frequency response method.

3.1 Large Eddy Simulation

LES, renowned for its accuracy in predicting fluid flow, can be used to simulate the unsteady flow field in furnace tubes (Métais, 2001; Temmerman et al., 2003; Tucker, 2014; Dong et al., 2018). The associated continuity and filtered N-S equations are (Zhang et al., 2014):

$$\partial \bar{u}_i / \partial x_i = 0 \tag{1}$$

$$\frac{\partial \bar{u}_i}{\partial t} + \frac{\partial \bar{u}_i \bar{u}_j}{\partial x_j} = \frac{\partial}{\partial x_j}\left[v\left(\frac{\partial \bar{u}_i}{\partial x_j} + \frac{\partial \bar{u}_j}{\partial x_i} \right) \right] - \frac{1}{\rho}\frac{\partial \bar{p}}{\partial x_i} - \frac{\partial \tau_{ij}}{\partial x_j}, \tag{2}$$

where $\bar{u}_i$ and $\bar{u}_j$ are the fluid velocity components (m/s); x_i and x_j represent the physical space (m); t is the time (s); v is the kinematic viscosity (m^2/s); p is the static pressure (Pa); ρ is the density (kg/m^3); and τ_{ij} is the subgrid-scale stress (Pa).

Equation (2) includes the subgrid-scale stress τ_{ij} (Shui et al., 2020), which can be calculated as follows based on the Smagorinshy-Lilly model (Basso et al., 2022):

$$\tau_{ij} - \frac{1}{3}\delta_{ij}\tau_{kk} = -2\mu_t \bar{S}_{ij}, \tag{3}$$

where δ_{ij} is the Kronecker Delta symbol; τ_{kk} is the isotropic part of the subgrid-scale stresses; μt is the subgrid-scale turbulent viscosity (m^2/s); and $\bar{S}_{ij}$ is the rate-of-strain tensor for the resolved scale. $\bar{S}_{ij}$ can be computed as:

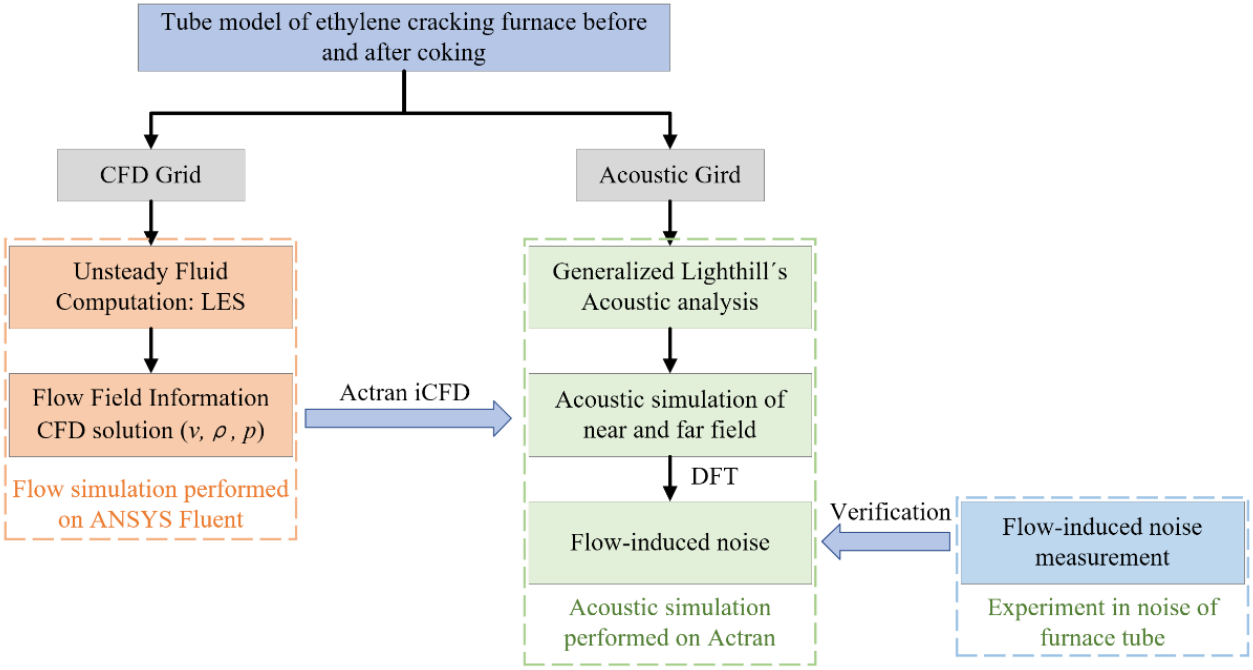

Fig. 2 Predicting flow-induced noise

$$\bar{S}_{ij} = \left(\partial \bar{u}_i / \partial x_j + \partial \bar{u}_j / \partial x_i\right) / 2. \tag{4}$$

In the Smagorinsky-Lilly model, the determination of the subgrid-scale turbulent viscosity μ_t is governed by Eqs. (5) to (7):

$$\mu_t = \rho L_s^2 \mid \bar{S} \mid \tag{5}$$

$$L_s = \min\left(kd, C_s V^{1/3}\right) \tag{6}$$

$$\mid \bar{S} \mid = \sqrt{2\bar{S}_{ij}\bar{S}_{ij}} \tag{7}$$

where L_s is the mixing length (m); k is the Von Karman constant, set to 0.42 in this case; d is the distance to the near wall (m); V is the volume of the computational cell (m^3); and C_s is the Smagorinsky constant.

To satisfy the Nyquist sampling theorem and ensure compatibility with the maximum acoustic frequency of interest, Eq. (8) should be aligned with the time step (Marzik et al., 2021):

$$\Delta t = \frac{1}{2 f_{\max}}, \tag{8}$$

where Δt is the time step size (s) and f_{max} is the maximum sampling frequency (Hz). To ensure numerical veracity and stability, the Courant number is normally required to meet the follow:

$$CFL = \frac{\Delta t \mid U \mid}{\Delta x} < 1, \tag{9}$$

where CFL is the Courant number; Δx is the cell size (m); and U is the flow velocity (m/s).

3.2 Generalized Lighthill's Acoustic Analogy

The proposed acoustic prediction model is founded on Goldstein's generalized Lighthill's acoustic analogy, with the equation derived from the N-S equation as follows: (Ki and Gil, 2020):

$$\frac{\partial^2 \rho'}{\partial t^2} - c_0^2 \nabla^2 \rho' = \frac{\partial^2 T_{ij}}{\partial x_i \partial x_j}, \tag{10}$$

where ρ_0 in $\rho'=\rho-\rho_0$ is the acoustic density disturbance (kg/m^3); c_0 is the ambient acoustic speed (m/s); and T_{ij} is Lighthill's stress tensor.

This equation only applies to free space, as it neglects the influence of the interaction between the fluid and the solid boundary on the acoustic field. Lighthill's equation for containing the stationary solid boundary in a fluid is as follows (Glegg & Devenport, 2017):

$$\begin{aligned} 4\pi c_0^2 \rho(\boldsymbol{x}, t) = & \frac{\partial^2}{\partial x_i \partial x_j} \iiint_{V_0} \frac{\left[T_{ij}\right]}{r} \mathrm{d}V(\boldsymbol{y}) \\ & + \frac{\partial}{\partial x_i} \iint_{\Sigma_0} \frac{n_j}{r} \left[\tau_{ij} + p\delta_{ij}\right] \mathrm{d}S(\boldsymbol{y}) \end{aligned} \tag{11}$$

The above derivation and solution can be employed when the fluid medium is stationary relative to the observer. However, in practical engineering problems, the flowing medium in the flow field moves constantly relative to the observer. The acoustic prediction model relies on Goldstein's generalized Lighthill acoustic analogy, an extension of Lighthill's theory that incorporates solid boundaries and the effects of a moving medium (Sun & Wang, 2021). Thus, the governing equation describing the acoustic field is:

$$\rho'(x,t) = \frac{1}{c_0^2}\int_{-T}^{T}\int_{v(\tau)}\frac{\partial^2 G}{\partial y_i \partial y_j}T_{ij}' dy d\tau + \frac{1}{c_0^2}\int_{-T}^{T}\int_{S(\tau)}\frac{\partial G}{\partial y_i} f_i dS(y) d\tau + \frac{1}{c_0^2}\int_{-T}^{T}\int_{S(\tau)}\rho_0 v_n' \frac{DG}{D\tau} dS(y) d\tau \quad , \tag{12}$$

where $x=[x_1, x_2, x_3]$ is a viewpoint; $y=[y_1, y_2, y_3]$ is an acoustic position; τ is emission time at the sound source (s); and G is the Green function.

3.3 Grid division and Boundary Conditions

Grids are primarily categorized as structured or unstructured. The former type exhibit high mesh quality, regular distribution of grid nodes, fast solution speed, and difficulty in applying complex models. The latter are easily operated and have wide adaptability, but lower solution accuracy. Given the relatively simple physical model of the research object in this study, and the need for precise calculation of the flow field in LES, fine grids are strictly required. Thus, ICEM was chosen to generate structured grids, as shown in Fig. 3(a).

Maintaining a $y^+<1$ criterion, the maximum grid size is 1×10^{-3} m, the first layer grid height is 3×10^{-6} m, and the grid growth ratio is 1.1, yielding a total of 20 layers and 1,380,060 grids. To ensure reliable acoustic calculation results, the acoustic field was meshed as shown in Fig. 3(b). A hybrid mesh of structured and unstructured elements was utilized. The maximum grid size is 3×10^{-3} m, with a total of 841,919 grids generated.

The furnace tube's inlet and outlet were set as the velocity inlet (V_{in}=10 m/s) and the pressure outlet, respectively. The ideal-gas law was applied for density calculations, and viscosity was determined using the Sutherland law (ANSYS, 2020). No-slip conditions were applied at the wall. The pressure-based implicit solver was employed for unsteady simulation, and the pressure-velocity coupling equation was solved using the Pressure Implicit with Splitting of Operator (PISO). Variables related to the control volume were interpolated using a second-order upwind scheme, and the standard wall function was applied for the near-wall grid nodes. The LES time step was set to 1×10^{-4} s, and the convergence criterion was set to an accuracy of 1×10^{-5}. The frequency resolution in the acoustic field is 25 Hz in this case.

3.4 Independence and Accuracy Verification

To strike a balance between computational accuracy and efficiency, independence and convergence tests were conducted on four different grids (Table 1). The pressure drop of the tube was selected as the importance index for the grid independence test in the flow field in this analysis, while OASPL was used as the grid-independent test standard. The grid convergence index (GCI) was used to evaluate grid convergence performance, with flow and acoustic field grid sizes set to 1×10^{-3} m and 3×10^{-3} m, respectively.

The ΔP value increases by 2.12 Pa, OASPL increases by 1.45 dB, and the errors are 0.3% and 1.2%, respectively. The slight changes indicate that the refined mesh can not only guarantee a sufficiently precise simulation but also minimizes computational cost, making it a preferred choice for this study. To validate the reliability and accuracy of the research method, experimental data from Lv and Ji (2011) was referenced and reproduced using the same method for comparison. As shown in Fig. 4, the simulation results are consistent with the experimental results. Consequently, this approach proves effective in predicting the flow-induced noise of furnace tubes both prior to and following coking.

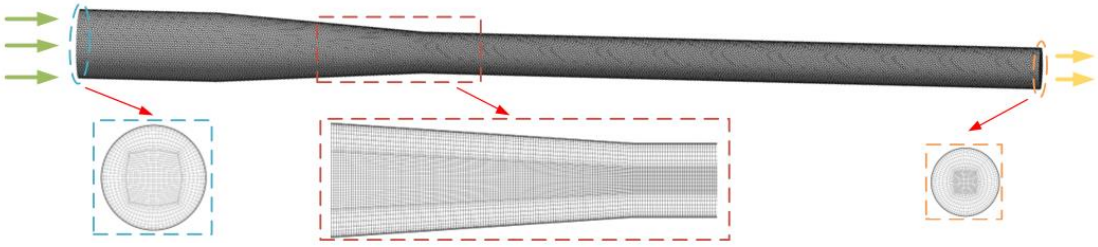

(a) Furnace tube geometry with the structured mesh in flow field

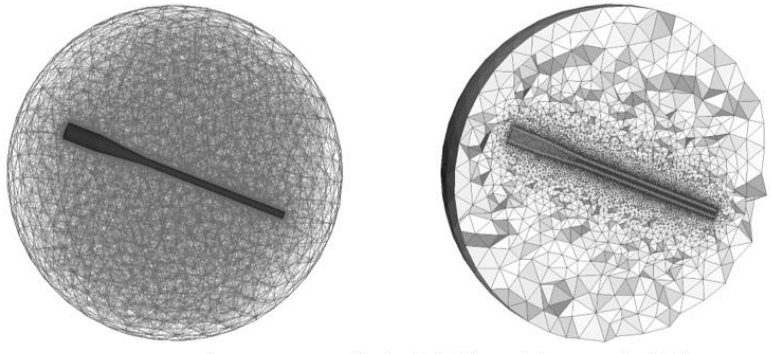

(b) Furnace tube geometry with the hybrid mesh in acoustic field

Fig. 3 Mesh generation of furnace tube geometry

Table 1 Validation of grid dependence

Grid type	N_{gird}[a]	N_{gird}[b]	Indicator of mesh refinement					
			ΔP (Pa)	Error (%)	GCI (%)	OASPL (dB)	Error (%)	GCI (%)
coarse	1268540	695211	630.94	/	/	108.75	/	/
original	1291541	748635	695.72	10.2	318.07	116.48	7.1	226.70
refined	1380060	841919	704.43	1.2	11.03	119.08	2.2	19.25
more refined	1580439	1068914	706.55	0.3	1.13	120.53	1.2	4.84

[a] N_{grid} is the number of flow field grids; [b] N_{grid} is the number of acoustic field grids;

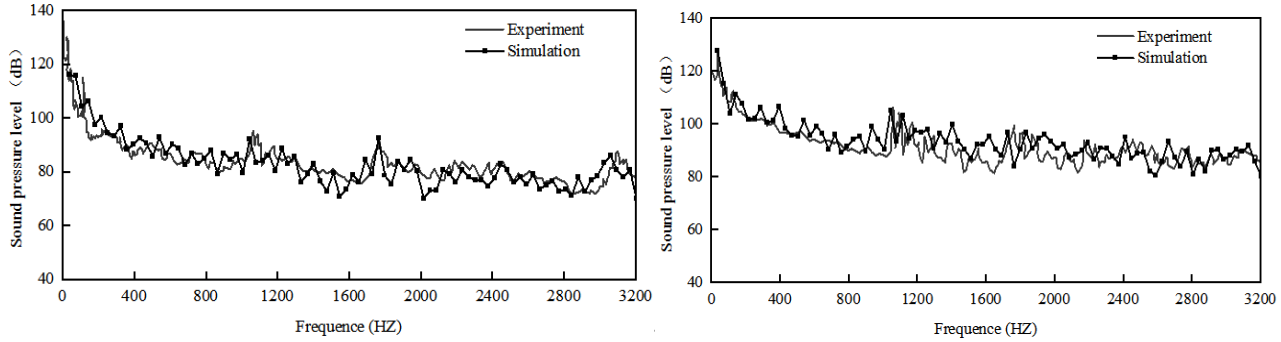

(a) Point 1 (b) Point 2

Fig. 4 Acoustic pressure spectrum curves with comparative experimental data (Lv & Ji, 2011)

4. RESULTS AND DISCUSSION

To investigate the flow-induced noise characteristics of the furnace tube before and after coking, acoustic field parameters at varying coke layer thicknesses (0 mm, 5 mm, 10 mm, and 15 mm) were examined. The analyzed parameters include experimental radiated power, radiated direction, surface sound power level, OASPL, and sound pressure spectrum. These parameter selections are grounded in relevant foundational theoretical principles in the field of fluid dynamics.

4.1 Experimental Radiated Power

Experimental radiated power represents the acoustic energy emitted by an acoustic source per unit of time, solely associated with the acoustic source itself. Figure 5 illustrates a comparison of the experimental radiated power 2 m away from the center of the ethylene cracking furnace tube across various coking degrees. The far-field experimental radiated power of the furnace tube before coking is extremely low, falling in the range of 0-2×10^{-6} W, at approximately 0 W. Conversely, in the coked furnace tube, the experimental radiated power increases with coke layer thickness, ranging from 0 W to 3 W. Thus, the far-field experimental radiated power of ethylene cracking furnace tubes under different coking degrees appears to be proportional to the thickness of the coke layer of tubes. This should provide a basis whether a coke layer is formed in the furnace tube.

Figure 5 also shows where the experimental radiated power of the ethylene cracking furnace tube with coke follows a normal distribution in the range of 0-2000 Hz, with noise energy predominantly concentrated in the 300-1500 Hz range. This indicates that the flow-induced noise resulting from coking primarily manifests as medium- and low-frequency noise when radiated to the far field. This finding aligns with observations by Ren et al. (2023). Additionally, as the coke layer increases, the frequency bands where the noise energy in the tube is mainly concentrated also form significant peak frequencies, namely, 794.56 Hz, 631.65 Hz, and 517.32 Hz.

4.2 Radiated Direction

To further investigate the noise characteristics induced by the flow in the coking tube, a total of 360 observation points were arranged around 2 m away from the center of the furnace tube to analyze the radiated direction of peak frequency, as depicted in Fig. 6. The inlet velocity of the furnace tube is 10 m/s in this case, and the thickness of the coke layer is 5 mm, 10 mm, or 15 mm. The peak frequency noise energy mainly radiates in the two directions of 150-210° and 330-30°, forming a distinctive Fig. 8 pattern. This radiation pattern aligns with the directivity characteristics associated with dipole acoustic sources (Sun & Wang, 2021).

The peak frequency sound pressure of the furnace tube further supports this finding, as shown in Fig. 7. Numerous sound sources (including dipoles and quadrupoles) appear to have formed in the furnace tube due to the influence of coking. However, it is evident that the sound source in the coked furnace tube becomes mainly dominated by dipoles as the coke layer thickens, while the energy radiated outward by the quadrupole sound source is negligible. This result aligns with Sujatha's (2023) research findings.

Moreover, although these monitoring points were 2 m away from the furnace tube (Fig. 6(a)), the maximum acoustic pressure level along the 10° direction still reaches 77 dB when coke layer thickness is 15 mm. This noise

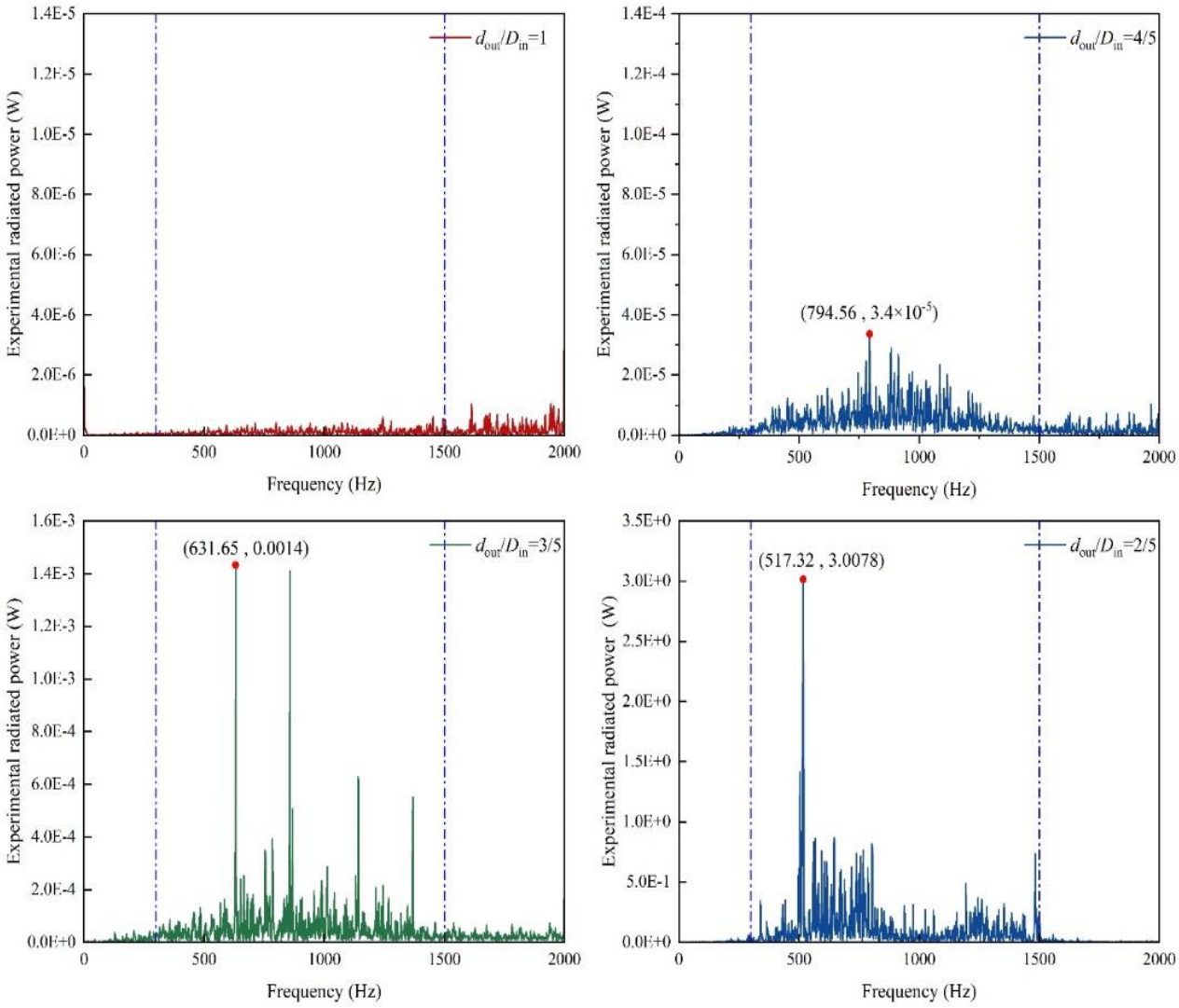

Fig. 5 Experimental radiated power at different coke layer thicknesses in furnace tubes

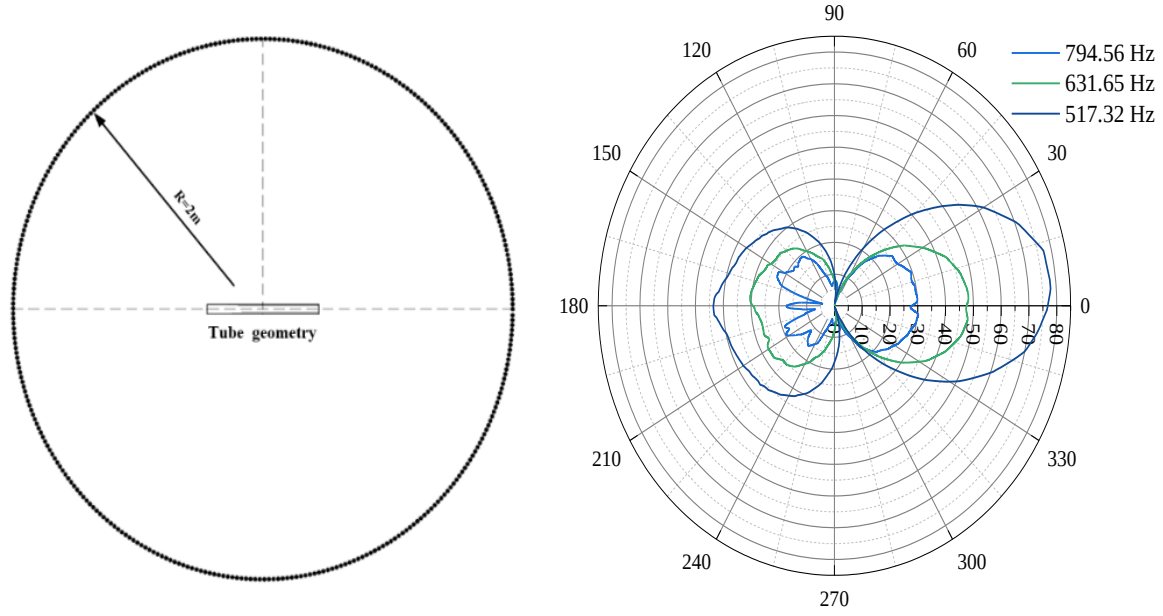

(a) Position of observation points (b) Sound pressure at different points

Fig. 6 Directivity of characteristic frequencies in far field

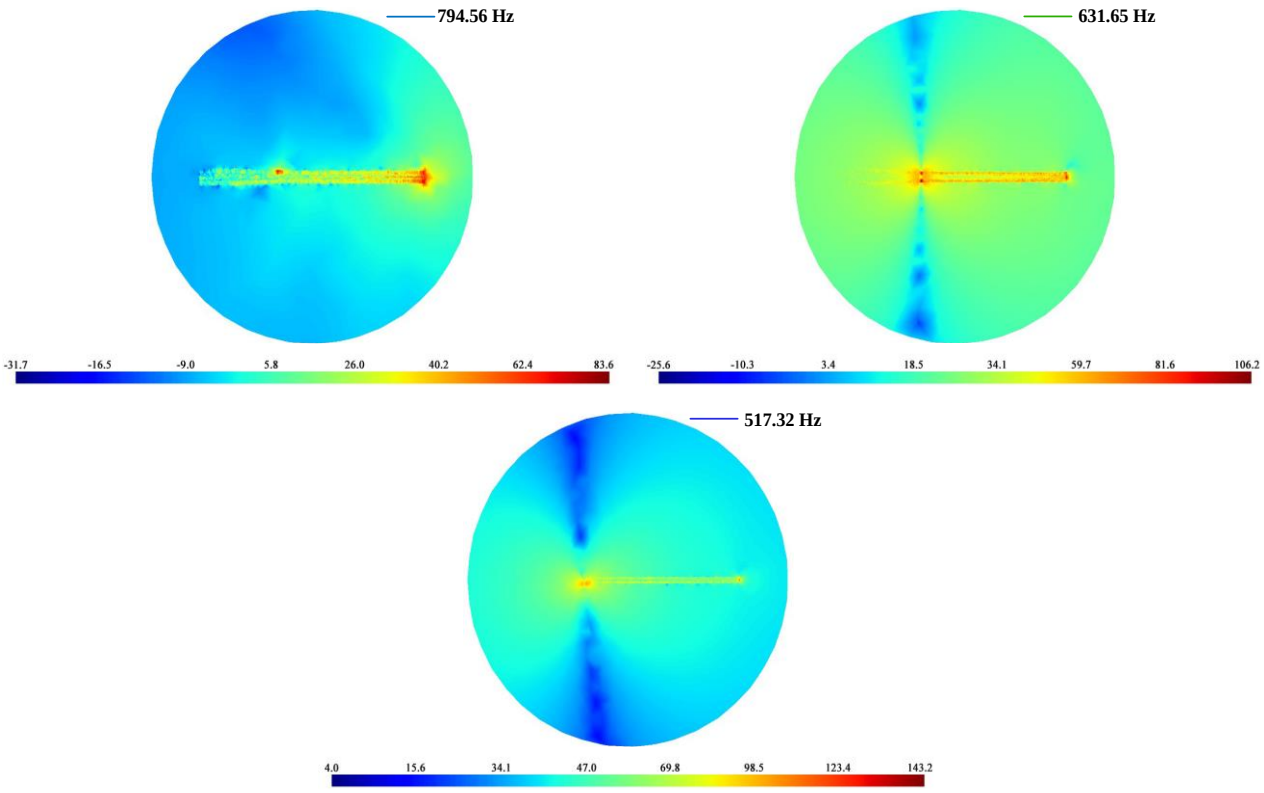

Fig. 7 Sound pressure at characteristic frequency in far field

level is far above the corresponding noise emission limit (Han et al., 2020).

4.3 Surface Sound Power Level

As outlined in Section 4.2, the primary noise source within the coked tube is the dipole acoustic source in the mid-low frequency band. It arises from the interaction force between the fluid and the inner wall boundary of the tube. The surface sound power level of the furnace tube was analyzed to gain a clearer understanding of its surface sound source distribution (Fig. 8). The sound power level distribution on the surface of the tube after coking is non-uniform, though this is the case with no coke deposition on the tube. Along the axial direction, the overall trend first decreases, then increases, then decreases, and finally stabilizes. The maximum sound power level differences between adjacent furnace tubes are 27.45%, 27.69%, and 26.5%. Along the radial direction, the overall change trend is characterized by increasing sound power level in the furnace tube with an increasing coke layer.

This phenomenon is both directly and indirectly related to the vorticity and turbulent intensity in the flow field, as shown in Fig. 9. The change trends of the two factors are very similar. Vorticity forms in the tube where the sound power on the surface of the furnace tube is relatively large (Fig. 9(a)), which implies that the turbulent flow in the furnace tube intensifies due to violent interactions among fluid molecules and a large local flow velocity gradient, mainly near the wall of the furnace tube and affected by the viscosity of the fluid itself. This viscosity is the primary contributor to dipole acoustic source generation, while the turbulence intensity on the inner wall of the furnace tube contributes to the surface sound power level (Moratilla et al., 2020).

Additionally, as evident in Fig. 9(b), the sound power level decreases from 53.15 dB to 48.04 dB at X=0.1 m, inversely proportional to the increase in coke layer thickness. Conversely, the sound power level increases from 51.40 dB to 105.03 dB at X=0.25 m, directly proportional to increasing coke layer thickness. Notably, the maximum sound power is located near the “necking” of the furnace tube after coking, indicating that this necking is the main source of noise. The inlet and outlet of the furnace tube are also important noise sources. The formation positions of these sound sources can also be observed in Fig. 7. Therefore, for the coked furnace tube, the distribution of the coke layer can be further judged based on the distribution of the surface sound power level.

4.4 Overall sound pressure level

The surface and far-field noise characteristics of the cracking furnace tube before and after coking were analyzed as discussed above; subsequently, the noise characteristics in the furnace tube were analyzed in further detail. The OASPL at each point on the central axis of the furnace tube was extracted to support this analysis, as illustrated in Fig. 10.

Overall, the OASPL of the noise caused by the flow in the furnace tube is proportional to the thickness of the coke layer. When coke layer thickness is 10 mm or 15 mm, the OASPL on the central axis of the furnace tube reaches the maximum at point (0.26, 0, 0) (near the necking of the tube), measuring 79.25 dB and 119.08 dB, respectively. Conversely, when the coke layer thickness is0 mm or 5

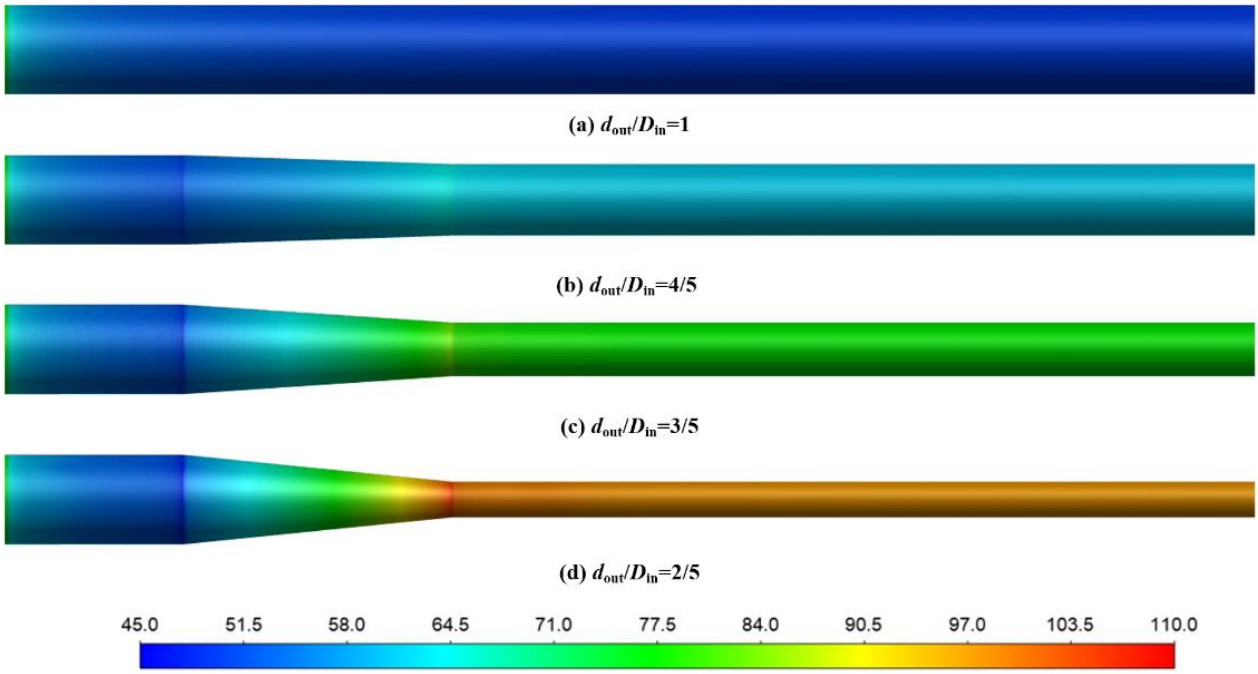

(a) Sound power level cloud

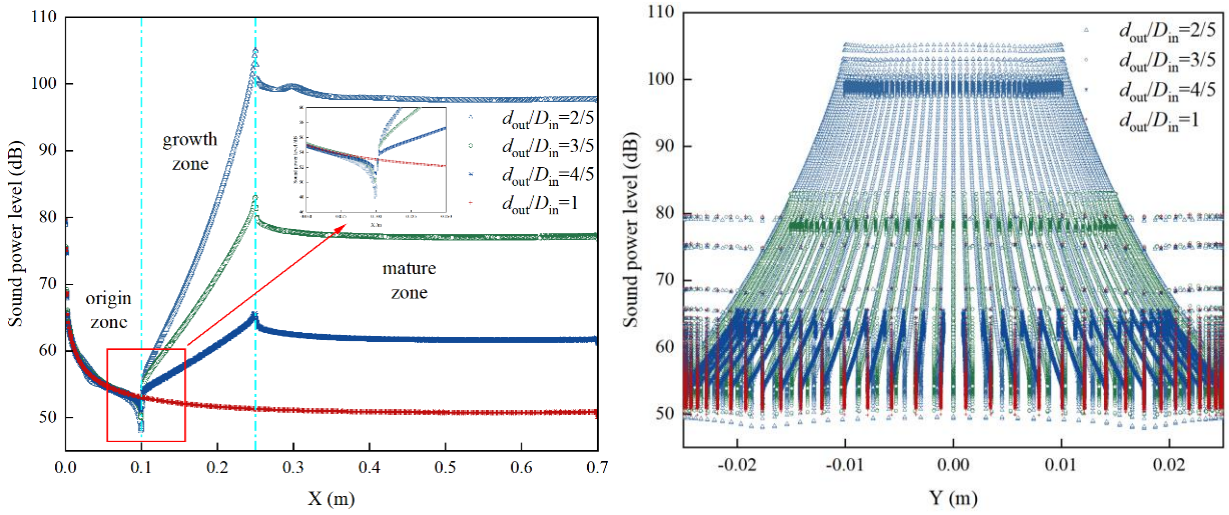

(b) Sound power level value

Fig. 8 Sound power level on surface of furnace tube

mm, the OASPL curve on the central axis of the furnace tube shows no obvious peak near this position. Therefore, furnace tubes with coke layers of different thicknesses attached to the inner wall can be classified according to the presence of a local peak in the OASPL curve on the central axis of the tube. This classification creates two working conditions: light coking and severe coking. On this basis, scientific and reasonable coke removal measures can be designated for the furnace tube.

Figure 10 also provides other valuable insights. Under light coking conditions, the OASPL along the central axis of the tube remains relatively consistent, displaying a gradual growth pattern. However, under heavy coking conditions, distinct trends emerge in different zones. In the origin and growth zones, the OASPL curve steadily increases; in the mature zone, the curve follows a pattern of a gentle linear decrease followed by a gradual increase. This phenomenon directly correlates with the flow dynamics in the furnace tube. As high-speed fluid is directed from a large-diameter tube to a small-diameter tube, the reduction in flow cross-sectional area increases local flow velocity and intensifies turbulence, thereby giving rise to significant pressure pulsations. These pressure pulsations, generated by the rapid fluid movement inside the furnace tube, play a prominent role in the generation of noise. Chen et al. (2021) made similar observations, highlighting the impact of flow dynamics on flow-induced noise in furnace tubes.

To provide a clearer explanation of the observed flow field phenomena and unveil the mechanism driving flow-induced noise in the furnace tube, the flow field in the tube with 15 mm coke layer thickness was isolated for further analysis. Six pressure pulsation monitoring points were arranged along the central axis of the tube to compare their

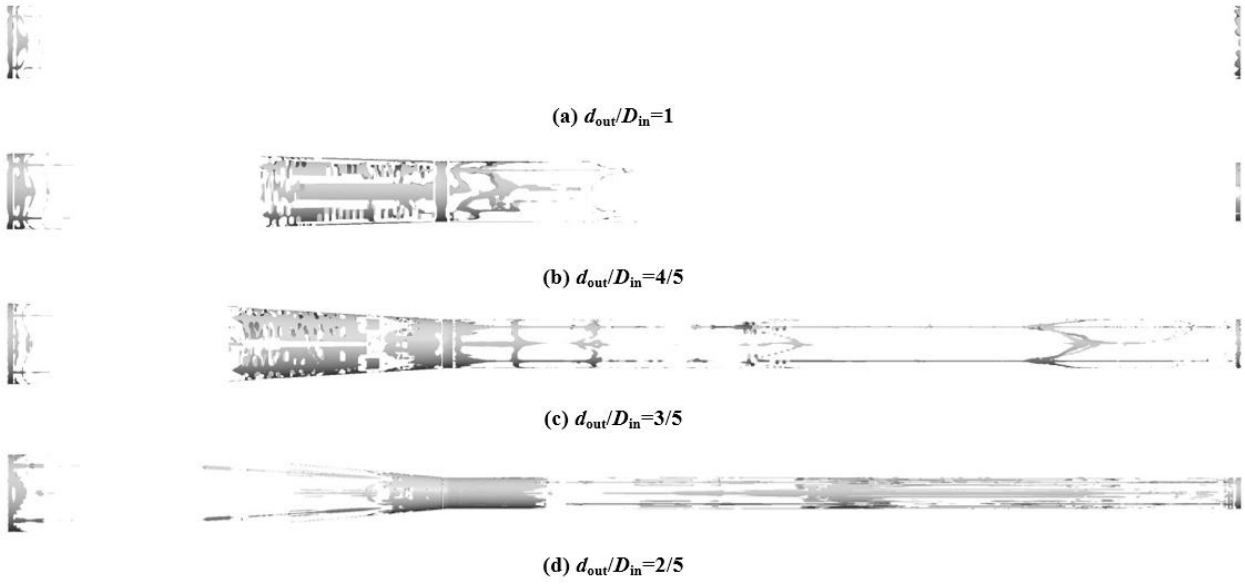

(a) vorticity cloud

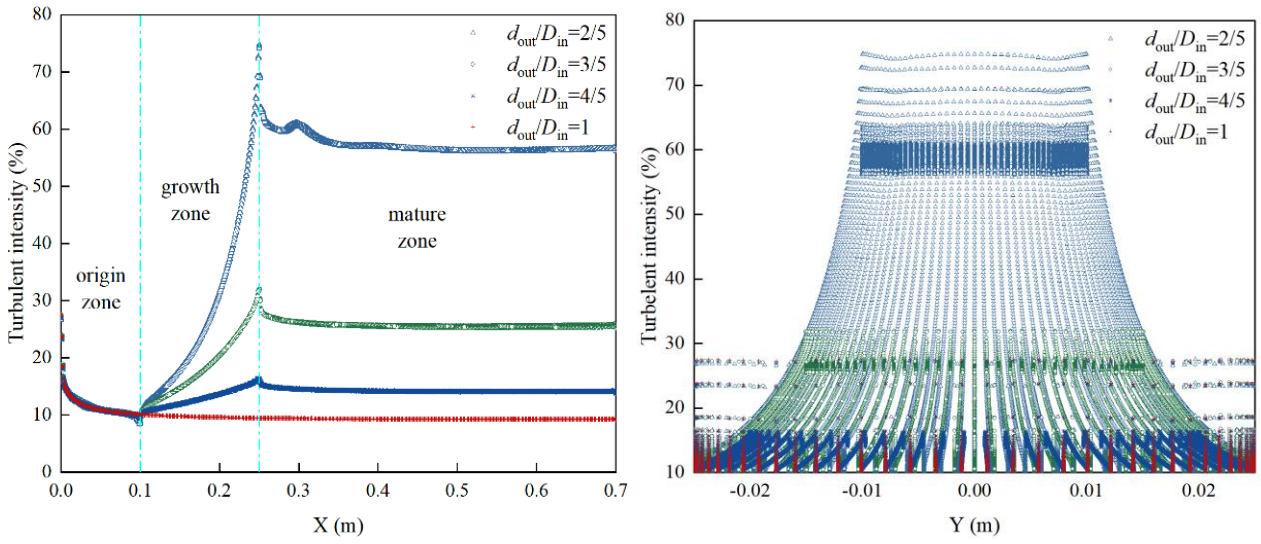

(b) turbulence intensity value

Fig. 9 Vorticity and turbulent intensity at different coke layer thicknesses in furnace tube

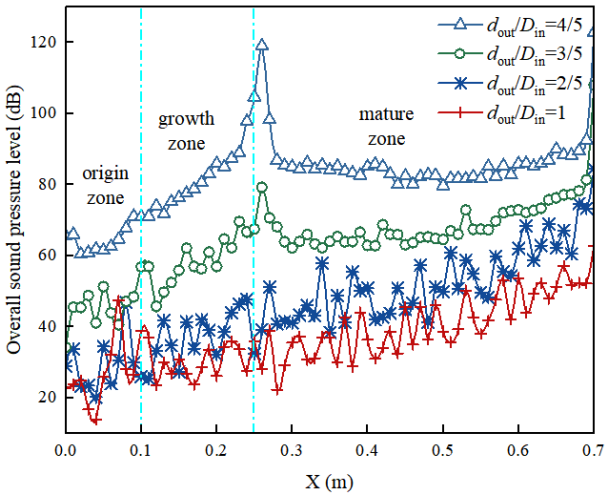

Fig. 10 Flow-induced noise on central axis of furnace tube

distribution characteristics along the flow direction, as illustrated in Fig. 11. In this coked furnace tube, the dimensionless coefficient of pressure pulsations peaks in the mature zone, surpassing that of the origin and growth zones. The pressure pulsation amplitude in the tube also reaches its maximum at the intersection of the growth and mature zones.

4.5 Sound Pressure Spectral

To evaluate the impact of noise from the flow in the furnace tube on the surrounding environment, the DFT was determined as a reflection of the sound pressure spectrum. Figure 12 shows where the noise inside the furnace tube exhibits broadband discrete noise characteristics (at point (0.35, 0, 0)) and outside the furnace tube (at points (2.35, 0, 0) and (0.35, 2, 0)). In addition, due to coke deposition, the sound pressure levels at the inner furnace tube point (0.35, 0, 0) vary

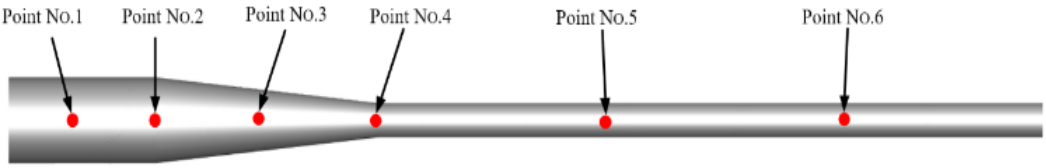

(a) Distribution of monitoring points in furnace tube

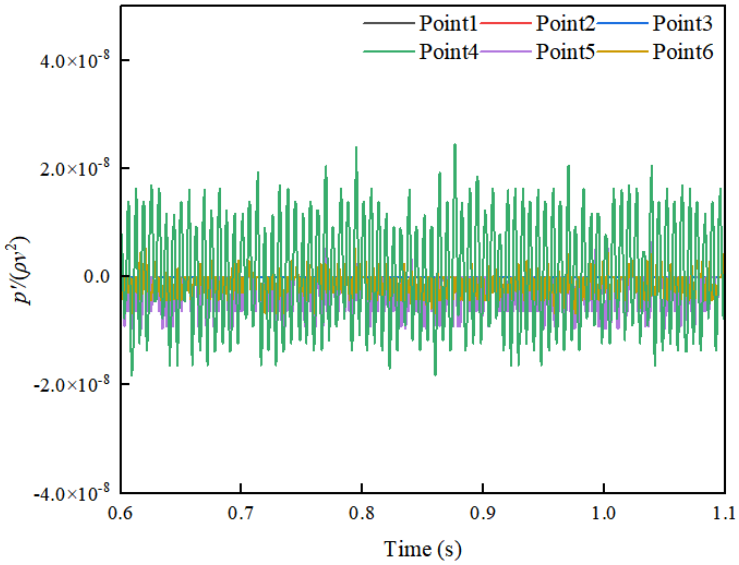

(b) Pressure fluctuation at monitoring points

Fig. 11 Flow field characteristics in furnace tube

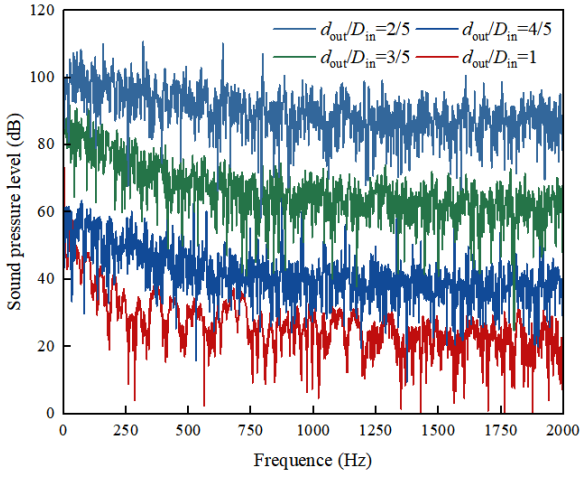

(a) Point (0.35, 0, 0)

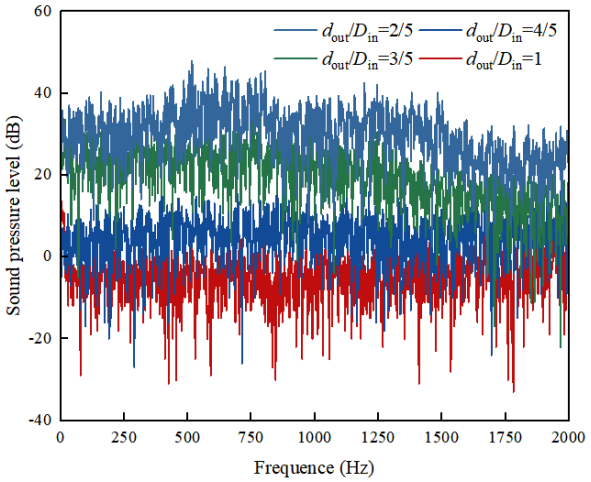

(b) Point (2.35, 0, 0)

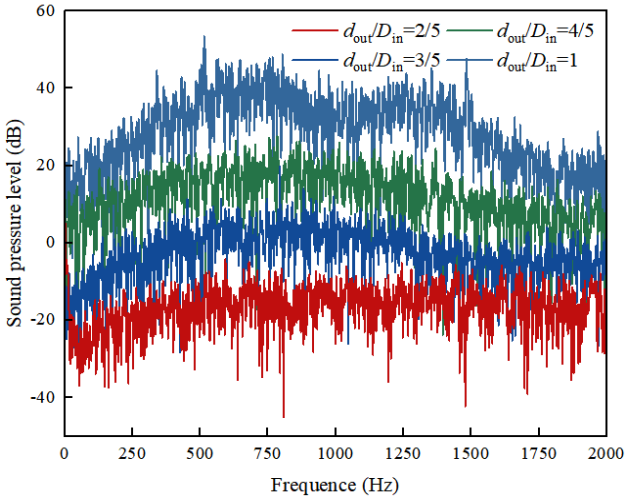

(c) Point (0.35, 2, 0)

Fig. 12 Spectral characteristics of near and far fields

significantly, unlike at outer tube points (2.35, 0, 0) and (0.35, 2, 0).

The sound pressure spectrum curve at point (0.35, 0, 0) of the furnace tube, both before and after coking, exhibits a decreasing trend in the 0-750 Hz range. The rate of attenuation is inversely proportional to the varying thickness of the coke layer within the furnace tube, as illustrated in Fig. 12. The sound pressure spectrum curve at point (2.35, 0, 0) shows a gentle growth trend in the range of 0-750 Hz. The sound pressure spectrum curve only attenuates in the range of 750-2000 Hz when the tube is heavily coked; this phenomenon is absent when the tube is lightly coked. Moreover, at point (0.35, 2, 0), there is a more pronounced change trend in the sound pressure spectrum curve.

5. CONCLUSION

To investigate the characteristics of flow-induced noise in ethylene cracking furnace tubes before and after coking, unsteady numerical simulations of furnace tube flow and acoustic fields were conducted in this study with coke layer thicknesses ranging from 0 mm to 15 mm. LES and a generalized Lighthill's acoustic analogy model were utilized. The analysis focused on the impact of coke deposition on flow-induced noise within the tube. The findings can be summarized as follows.

(1) The far-field experimental radiated power of ethylene cracking furnace tubes at various coking degrees predominantly manifests in the frequency range of 300-1500 Hz, portraying characteristics of medium- and low-frequency noise. The magnitude of this noise exhibited a direct correlation with coke layer thickness.

(2) Numerous dipole and quadrupole sound sources are generated within the coked tube, influenced by viscosity, depicted as turbulence intensity and vorticity in this study. These sources are primarily concentrated in the necking region, as well as the inlet and outlet of the tube.

(3) With coke layer thicknesses of 5 mm, 10 mm, and 15 mm, the energy radiated by the sound source within the furnace tube concentrates at frequencies of 794.56 Hz, 631.65 Hz, and 517.32 Hz, respectively. These frequencies predominantly exhibit dipole sound source characteristics. Radiation energy from quadrupole sound sources is negligible in the far field.

(4) The coking degree of the furnace tube can be determined based on the presence or absence of a local peak in the total sound pressure level curve along its central axis. This classification creates two operational conditions: mild coking and severe coking. Such categorization provides a foundation for implementing appropriate coking measures for the furnace tube based on scientific principles.

ACKNOWLEDGEMENTS

This work was sponsored by the Postgraduate Research &Practice Innovation Program of Jiangsu Province [grant number KYCX22_3119], Natural Science Research Project of Colleges and Universities of Jiangsu Province [grant number 20KJA470001], the China National Petroleum Corporation &Innovation Consortium Science and Technology Cooperation Project of Changzhou University [grant number KYZ22020129].

CONFLICT OF INTEREST

It is declared here that there are no known competing financial interests or personal relationships among the authors that could have appeared to influence the work reported in this study.

AUTHORS CONTRIBUTION

F. Q. Zhou: Conceptualization, Methodology, Funding acquisition, Project administration; **S. Y. Zhao**: Writing Original Draft, Visualization, Data Curation; **S. J. Zhang**: Writing Review & Editing, Supervision, Resources, Validation, Investigation, Formal analysis, Data curation; **Y. Zhang**: Funding acquisition, Project administration; **S. C. Fu**: Funding acquisition, Project administration; **S. Q. Yu**: Funding acquisition, Project administration, Validation, Investigation.

REFERENCES

Amini, E., Peyghambarzadeh, S. M., Zarrinabadi, S., & Hashemabadi, S. H. (2022). Simulation of heat transfer and fluid flow of hot oil in radiation section of an industrial furnace considering coke deposition. *Journal of Thermal Analysis and Calorumetry*, *147*(14), 4821-4835. https://doi.org/10.1007/s10973-021-10847-7.

ANSYS, *ANSYS 2020 R2 Theory Guide* (2020). Technical Report. ANSYS Fluent Theory Guide, V.20.2.

Barik, A. K., Satapathy, P. K., & Sahoo, S. S. (2016). CFD study of forced convective heat transfer enhancement in a 90° bend duct of square cross section using nanofluid. *Sādhanā*, *41*(7), 795-804. https://doi.org/10.1007/s12046-016-0507-6.

Basso, F. O., Franco, A. T., & Pitz, D. B. (2022). Large-eddy simulation of turbulent pipe flow of Herschel-Bulkley fluids-Assessing subgrid-scale models. *Computers & Fluids*, *224*, 105522. https://doi.org/10.1016/j.compfluid.2022.105522.

Haldar, B., & Shukla, A. (2017). A Review on heat transfer and fluid flow within u-pipe and bend pipe. *Engineering-PRC*, *3*(4), 319-325. https://doi.org/10.23883/ijrter.2017.3152.dnxrh.

Chen, G., Liang, X. F., Zhou, D., Li, X. B., & Lien, F. S. (2021). Numerical study of flow and noise predictions for tandem cylinders using incompressible improved delayed detached eddy simulation combined with acoustic perturbation equations. *Ocean Engineering*, *224*, 108740. https://doi.org/10.1016/j.oceaneng.2021.108740.

Chen X. Q., Luo Y., Chen Y. K., & Long L. (2023). Failure analysis of overheated coil leakage in ethylene cracking furnace. *Engineering Failure*

Analysis, *152*, 10746. https://doi.org/10.1016/j.engfailanal.2023.107465.

Coombs, J. L., Schembri, T. J., & Zander, A. C. (2020). Pipeline blowdown noise levels and noise modelling. *Applied Acoustic*, *168*, 107405. https://doi.org/10.1016/j.apacoust.2020.107405.

Dong, Q. L., Xu, H. Y., & Ye, Z. Y. (2018). Numerical investigation of unsteady flow past rudimentary landing gear using DDES, LES and URANS. *Engineering Applications of Computational Fluid Mechanics*, *12*(1), 689-710. https://doi.org/10.1080/19942060.2018.1510791.

Fakhroleslam, M., & Sadrameli, S. M. (2020). Thermal cracking of hydrocarbons for the production of light olefins; a review on optimal process design, operation, and control. *Industrial & Engineering Chemistry Research*, *59*(27), 12288-12303. https://pubs.acs.org/doi/10.1021/acs.iecr.0c00923.

Glegg, S., & Devenport, W. (2017). Chapter 4 - Lighthill's acoustic analogy. In Glegg, S. & Devenport, W. (Eds.), Aeroacoustics of Low Mach Number Flows (pp. 73-79) *Academic Press*. https://doi.org/10.1016/B978-0-12-809651-2.00004-7.

Han, T., Wang, L., Cen, K., Song, B., Shen, R. Q., Liu, H. B., & Wang, Q. S. (2020). Flow-induced noise analysis for natural gas manifolds using LES and FW-H hybrid method. *Applied Acoustic*, *159*, 107101. https://doi.org/10.1016/j.apacoust.2019.107101.

Han, Z. Y., Xie, G. S., Cao, L. W., & Sun, G. H. (2019). Material degradation and embrittlement evaluation of ethylene cracking furnace tubes after long term service. *Engineering Failure Analysis*, *97*, 568-578. https://doi.org/10.1016/j.engfailanal.2019.01.041.

IEA. (2021). *Global Energy Review 2021*. IEA, Pairs. https://www.iea.org/reports/global-energy-review-2021.

Jakobi, D., & Gommans, R. (2007). Corrosion by carbon and nitrogen. In H. J. Grabke & M Schütze (Eds.), *Typical failures in pyrolysis coils for ethylene cracking* (pp. 259-270). European Federation of Corrosion (EFC) Series. https://doi.org/10.1533/9781845693350.259.

Ki, H. K., & Gil, H. Y. (2020). Aeroacoustic topology optimization of noise barrier based on Lighthill's acoustic analogy. *Journal of Sound and Vibration*, *483*, 115512. https://doi.org/10.1016/j.jsv.2020.115512.

Lv, F. R., Wang, M., Zhe, C. T., Guo, C., & Gao, M. (2023). Numerical simulation of 3D flow field and flow-induced noise characteristics in a T-Shaped reducing tee junction. *Fluid Dynamics & Materials Processing*, *19*(6), 1463-1478. https://doi.org/10.32604/fdmp.2023.024259.

Lv, J. W., & Ji, Z. L. (2011). Numerical prediction and experimental measurement of flow noise in variable cross-sectional area pipes. *Noise and Vibration Control*, *31*(1), 166-169. https://nvc.sjtu.edu.cn/CN/Y2011/V31/I1/166.

Mahamulkar, S., Yin, K. H, Agrawal, P. K., Davis, R. J., Jones, C. W., Malek, A., & Shibata, H. (2016). Formation and oxidation/gasification of carbonaceous deposits: A review. *Industrial & Engineering Chemistry Research*, *55*(37), 9760-9818. https://doi.org/10.1021/acs.iecr.6b02220.

Marzik, G., Sato, S. I., & Girola, M. E. (2021). Compressive sensing for perceptually correct reconstruction of music and speech signals. *Applied Acoustic*, *183*, 108328. https://doi.org/10.1016/j.apacoust.2021.108328.

Métais, O. (2001). Large-eddy simulations of turbulence. In M. Lesieur, A. Yaglom & F. David (Eds.), *New trends in turbulence Turbulence: nouveaux aspects* (pp. 113-186). Springer, Berlin, Heidelberg. https://doi.org/10.1007/3-540-45674-0_3.

Mohammed, A. (2018). CFD analysis for turbulent flow and heat transfer in U-Tube. *Journal of Engineering and Applied Sciences*, *13*, 11122-11134. DOI:10.3923/jeasci.2018.11122.11134.

Moratilla-Vega, M. A, Lackhove, K., Janicka, J., Xia H., & Page, G. J. (2020). Jet noise analysis using an efficient LES/high-Order acoustic coupling method. *Computers & Fluids*, *199*, 104438. https://doi.org/10.1016/j.compfluid.2020.104438.

Mori, M., Masumoto, T., & Ishihara, K. (2017). Study on acoustic, vibration and flow induced noise characteristics of T-shaped pipe with a square cross-section. *Applied Acoustics*, *120*, 137-147. DOI:10.1016/j.apacoust.2017.01.022.

Murugu, S. P., Srikrishnan, A. R., Krishnaraj, B. K., Jayaraj, A., Mohammad, A., & Velamati, R. K. (2022). Acoustic Modeling of Compressible Jet from Chevron Nozzle: *A Comparison of URANS, LES and DES Models. Symmetry*, *14*(10), 1975. https://doi.org/10.3390/sym1410197.

Pan, F. H., & Lan, J. J. (2016, April). *Analysis on Influence of Environmental Factors to the Heat Loss of Petrochemical Heating Furnace Wall*. 6th International Conference on Electronic, Mechanical, Information and Management Society, Shenyang, China. https://doi.org/10.2991/emim-16.2016.211.

Paul, C., Mahmoud, K., & Nicole, K. (2018, November). *A computationally efficient approach to predict the acoustic fields from a cylinder in cross flow*. INTER-NOISE and NOISE-CON Congress and Conference Proceedings, Institute of Noise Control Engineering, Ibiza, Spain. https://www.ingentaconnect.com/content/ince/incecp/2018/00000257/00000001/art00088.

Pittard, M. T., Evans, R. P., Maynes, R. D., & Blotter, J. D. (2004). Experimental and numerical investigation of turbulent flow induced pipe vibration in fully developed flow. *Review of Scientific Instruments*, *75*(7), 2393-2401.

https://doi.org/10.1063/1.1763256.

Ren, C. X., Ye, M. L., Wang, X. W., Dong, Z. Q., & Kang, H. C. (2020). Energy saving analysis of mechanical coke cleaning and chemical cleaning for cracking furnace. *Ethylene Industry (China)*, *32*(03), 39-41. https://qikan.cqvip.com/Qikan/Article/Detail?id=7102878143.

Ren, Y., Qin, Y. X., Pang, F. Z., Wang, H. F., Su, Y. M., & Li, H. C. (2023). Investigation on the flow-induced structure noise of a submerged cone-cylinder-hemisphere combined shell. *Ocean Engineering*. *270*, 113657. https://doi.org/10.1016/j.oceaneng.2023.113657.

Rossi, F., Rovaglio, M., & Manenti, F. (2019). Mathematical modelling of gas-phase complex reaction systems: Pyrolysis and combustion. In T. Faravelli, F. Manenti & E. Ranzi (Eds.), *Model predictive control and dynamic real-time optimization of steam cracking units* (pp. 873-897). Computer Aided Chemical Engineering. https://doi.org/10.1016/B978-0-444-64087-1.00018-8.

Shui, Q. X., Duan, C. E., Wu, X. Y., Zhang, Y. W., Luo, X. L., Hong, C., He Y. P., Wong, N. H., & Gu Z. L. (2020). A hybrid dynamic Smagorinsky model for large eddy simulation. *International Journal of Heat and Fluid Flow*, *86*, 108698. https://doi.org/10.1016/j.ijheatfluidflow.2020.108698.

Solaimany Nazar, A. R., Banisharifdehkordi, F., & Ahmadzadeh, S. (2016). Mathematical modeling of coke formation and deposition due to thermal cracking of petroleum fluids. *Chemical Engineering & Technology*, *39*(2), 311-321. https://doi.org/10.1002/ceat.201400528.

Su, X., Wu, Y., Pei, H., Gao, J., & Lan, X. Y. (2016). Prediction of coke yield of FCC unit using different artificial neural network models. *China Petroleum Processing and Petrochemical Technology*, *18*, 102-109. https://www.researchgate.net/publication/311603565.

Sun, X. F., & Wang, X. Y. (2021). *Fundamentals of Aeroacoustics with Applications to Aeropropulsion Systems*. Shanghai Jiao Tong University Press Aerospace Series. https://doi.org/10.1016/C2012-0-02671-3.

Sujatha, C. (2023). *Fundamentals of Acoustics*. Vibration, Acoustics and Strain Measurement. https://doi.org/10.1007/978-3-031-03968-3_4.

Tari, V., Najafizadeh, A., Aghaei, M. H., & Mazloumi, M. A. (2009). Failure analysis of ethylene cracking tube. *Journal of Failure Analysis and Prevention*, *9*(4), 316-322. https://doi.org/10.1007/s11668-009-9259-5.

Temmerman, L., Leschziner, M. A., Mellen, C. P., & Fröhlich, J. (2003) Investigation of wall-function approximations and subgrid-scale models in large eddy simulation of separated flow in a channel with streamwise periodic constrictions. *International Journal of Heat and Fluid Flow*, *24*(2), 157-180. https://doi.org/10.1016/S0142-727X(02)00222-9.

Tucker, P. G. (2014). *Turbulence and Its modelling*. Unsteady Computational Fluid Dynamics in Aeronautics. Springer, Dordrecht. https://doi.org/10.1007/978-94-007-7049-2_3.

Valus, M. G., Fontoura, D. V. R., Serfaty, R., & Nunhez, J. R. (2017). Computational fluid dynamic model for the estimation of coke formation and gas generation inside petrochemical furnace pipes with the use of a kinetic net. *The Canadian Journal of Chemical Engineering*, *95*(12): 2286-2292. https://doi.org/10.1002/cjce.23007.

Wei, Y. R. (2020). Application and discussion of mechanical decoking technology of furnace. *Petroleum Refinery Engineering*, *50*(08), 22-25. DOI: 10.3969/j.issn.1002-106X.2020.08.006.

Zhang, N., Qiu, T., & Chen, B. Z. (2013). CFD simulation of propane cracking tube using detailed radical kinetic mechanism. *Chinese Journal of Chemical Engineering*, *21*(12), 1319-1331. https://doi.org/10.1016/S1004-9541(13)60619-9.

Zhang, Y., Miao, Y., Zhang, S. Y., & Zhou, F. Q. (2023). Numerical simulation of acoustic field characteristics of flow-induced noise by coking on inner wall of furnace tube. *Journal of Safety and Environment*, *8*, 1-10. DOI:10.13637/j.issn.1009-6094.2023.0868.

Zhang, Y. O., Zhang, T., Ouyang, H., & Li, T. Y. (2014). Flow-induced noise analysis for 3D trash rack based on LES/Lighthill hybrid method. *Applied Acoustic*, *79*, 141-152. https://doi.org/10.1016/j.apacoust.2013.12.016.